Inorganic Chemistry

Article

pubs.acs.org/IC

Endo- and Exocyclic Supramolecular Complexes of Mixed-Donor Macrocycles via [1:1] and [2:2] Cyclizations

Seul-Gi Lee,[†] Ki-Min Park,[†] Yoichi Habata,[‡] and Shim Sung Lee*[,†]

[†]Department of Chemistry and Research Institute of Natural Science, Gyeongsang National University, Jinju 660-701, South Korea

[‡]Department of Chemistry, Toho University, 2-2-1 Miyama, Funabashi, Chiba 274-8510, Japan

Supporting Information

ABSTRACT: A 20-membered $N_2O_2S_2$ macrocycle ($\mathbf{L^1}$) and a 40-membered $N_4O_4S_4$ macrocycle ($\mathbf{L^2}$) obtained from the mixed products via respective [1:1] and [2:2] cyclization are employed, and a comparative investigation of the coordination behavior of these macrocyclic ligands with nickel(II), cadmium(II), and silver(I) is reported. The X-ray structures of seven complexes (**1**−**7**) have been determined, and a range of structural types and coordination modes, including mono- to multinuclear and endo- to exocyclic coordination, is presented. The cation-dependent endocyclic 1:1 (metal-to-ligand) complex $[Ag(\mathbf{L^1})]NO_3$ (**1**) and a sandwich-like 1:2 $[Cd(\mathbf{L^1})_2](NO_3)_2$ (**2**) complex exhibiting different stoichiometries and metal positions in the complexes were obtained by the reactions of the smaller macrocycle $\mathbf{L^1}$ with $AgNO_3$ and $Cd(NO_3)_2$, respectively. Meanwhile, the reactions of $\mathbf{L^1}$ with $Ni(ClO_4)_2{\cdot}6H_2O$ and $Ni(NO_3)_2{\cdot}6H_2O$ afforded the anion-dependent perching-type mononuclear solvato-complex $[Ni(\mathbf{L^1})(CH_3CN)_3](ClO_4)_2{\cdot}2CH_3CN$ (**3**) and the sandwich-like complex $[Ni(\mathbf{L^1})_2(NO_3)_2]$ (**4**), respectively. In the complexations of the larger macrocycle $\mathbf{L^2}$ with $AgNO_3$, two endocyclic dinuclear complexes $[Ag_2(\mathbf{L^2})(CH_3CN)_2](NO_3)_2$ (**5**) and $[Ag_2(\mathbf{L^2})](NO_3)_2$ (**6**) with different coordination environments were isolated as a kinetic (**5**) and thermodynamic controlled (**6**) products in neutral condition. The identical reaction in acidic condition afforded a stairtype one-dimensional (1-D) coordination polymer $\{[Ag_2(H_4\mathbf{L^2})(\mu_2\text{-}NO_3)(NO_3)_2](NO_3)_3{\cdot}CH_3CN{\cdot}3H_2O\}_n$ (**7**) in which the disilver(I) complex cation units are connected by nitrate ions. From these results, the effects of the cation, anion, and size ratio on the topologies of the resulting solid complexes are discussed. NMR titrations of $\mathbf{L^1}$ and $\mathbf{L^2}$ with silver(I) nitrate were also carried out to explore their complexation behaviors in solution and for comparison with the solid state structures.

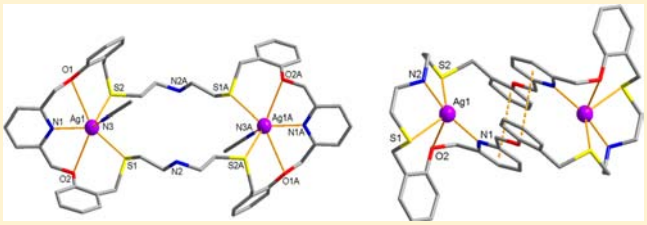

INTRODUCTION

There is a growing interest in a large macrocyclic ligand system that can form binuclear complexes exhibiting electron transport, charge transfer, and allosteric behavior.[1,2] Therefore, design and synthesis of new macrocyclic ligand systems capable of forming binuclear complexes have received considerable attention. The macrocyclic ligand synthesized via a 2:2 cyclization has a large cavity that can bind two metal ions in the defined position. Since most large macrocycles based on the 2:2 cyclization reported are the Schiff base type, their dinuclear complexes have been focused on the transition metal ions.[1] Reduction of such Schiff base species sometimes provides the synthesis of large flexible macrocycles comprising di- or multinuclear binding sites. For the non-Schiff base type macrocycles including the cyclam and related large ring types, a number of dinuclear transition metals and silver(I) complexes have been known.[4]

For non-Schiff base type large thiamacrocycles, reaction between a dithiol and a dihalide or ditosylate gives a 2:2 cyclization product with a large ring cavity in which two dithiol and two dihalide groups are circulated by four C−S bond formations.[2,3] Habata et al.[2b] have reported the synthesis of the N_2S_6 macrocycle with a 24-membered ring cavity via 2:2 dithiol-dihalide cyclization and its disilver(I) complex.

We have been involved in a program of preparing a new type of dinuclear macrocyclic complex based on a mixed-donor thimacrocyclic system including large macrocycles,[3] linked macrocycles,[5] endo/exodentate macrocycles,[6] and calix-bis-crowns.[7] Recently, we have reported the synthesis of an extra large 40-membered $N_4O_4S_4$ macrocycle $\mathbf{L^2}$ as a 2:2 dithiol-dichloride cyclization product and its 1:1 cyclization analogue $\mathbf{L^1}$ (20-membered), and their mono- and dimercury(II) complexes,[3] respectively (Chart 1). The continuing interest in the large thiamacrocycles which can adopt dinuclear complexes and the relatively little research in this area motivated us to extend these studies employing the soft metal system.

Herein, we report the synthesis and structural charaterization of nickel(II), cadmium(II), and silver(I) complexes with a 20-membered $N_2O_2S_2$ macrocycle ($\mathbf{L^1}$) and a 40-membered $N_4O_4S_4$ macrocycle ($\mathbf{L^2}$) obtained from the mixed products via [1:1] and [2:2] cyclization, along with discussion of the comparative coordination behavior of these macrocyclic ligands. In addition, NMR and ESI mass studies for the formations of the mono- and disilver(I) complexes with the smaller and larger macrocycles are

Received: February 1, 2013
Published: July 25, 2013

dx.doi.org/10.1021/ic400247q | Inorg. Chem. 2013, 52, 8416−8426

Chart 1. A 20-Membered (L^1) and a 40-Membered (L^2) Macrocycles Used in This Work

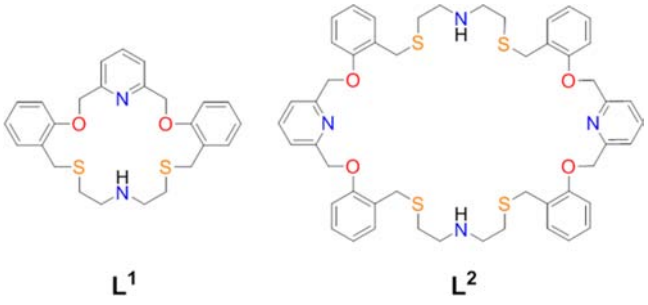

also reported. In this work, the larger macrocycle via non-Schiff base [2:2] cyclization represents the potential to provide a wide range of binding properties aimed not only at obtaining new types of binuclear species but also at preparing metallo-supramolecular networks.

RESULTS AND DISCUSSION

The smaller (L^1) and the larger (L^2) macrocycles were prepared by 1:1 and 2:2 cyclization reactions utilizing *N*-Boc-protected dithiol and corresponding dichloride, and isolated from its resuling binary macrocycles mixture as described previously by us.[3] A comparative study of the interactions of these macrocycles with the soft metal salts has been carried out and discussed in terms of cation, anion, and cavity size both in solid and solution states.

Cation-Dependent Silver(I) and Cadmium(II) Nitrate Complexes of L^1 (1 and 2). In an attempt to compare the reactivity of silver(I) and cadmium(II) as d^{10} soft metal ions toward the smaller macrocycle L^1, the cation-dependent products **1** and **2** with different stoichiometries and metal ion positions in the complexes were obtained as depicted in Scheme 1. Each structure was characterized by single crystal X-ray analysis (Figure 1).

With complexations of L^1 with the d^{10} metal ion (Ag^+ and Cd^{2+}) nitrates, we were able to prepare one typical endocyclic 1:1 (metal-to-ligand) complex $[Ag(L^1)]NO_3$ (**1**) (Figure 1a) and one exocyclic 1:2 complex $[Cd(L^1)_2(NO_3)_2]$ (**2**) (Figure 1b). Selected geometric parameters of **1** and **2** are presented in Table 1.

Scheme 1. Cation-Dependent Endocyclic 1:1 (1) and Exocyclic 1:2 (2) Metal Nitrate Complexes of L^1

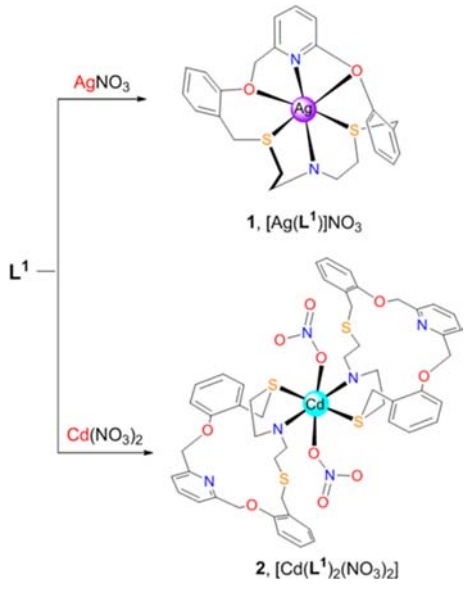

In **1**, the silver(I) center in a cavity is six-coordinate, being bound to all donor atoms from L^1, adopting a "tight-and-twisted" conformation. In this structure, the silver(I) center is shielded from further interactions with anion and solvent by the ligand with the twisted conformation due to its slightly larger cavity size (20-membered) compared to that of the central metal ion: silver(I) is known to best fit the 18-membered cavity. Thus, unlike most of macrocyclic silver(I) nitrate complexes,[8] the anion in **1** remains uncoordinated. The Ag–S bond distances in **1** [Ag1–S1, 2.648(1), Ag1–S2, 2.642(1) Å] are typical, and those of the Ag–O bonds [Ag1–O1 2.952(2) and Ag1–O2 2.904(2) Å] show somewhat elongated lengths[8,9] because of the larger macrocyclic cavity size for the silver(I) encirculation. The pyridine nitrogen in **1** appears to bind strongly to the silver(I) center [Ag1–N1 2.342(2) Å] which is slightly shorter than that of the secondary amine nitrogen [Ag1–N2, 2.419(2) Å], both of which are within the normal range for these bond types.[8c] The silver(I) coordination in **1** cannot be described simply in terms of a regular geometry. Consequently, the preferred endocyclization toward silver(I) without anion coordination in **1** presumably reflects the overall strong coordination of the donor-set of highly twisted L^1 in the 3D conformation.

In **2**, the cadmium(II) which lies outside the cavity is sandwiched by two macrocycles. The cadmium(II) is six-coordinate, being bound to one sulfur and one secondary nitrogen donor from each L^1. The coordination sphere in **2** is completed by two monodentate nitrato ligands with one pyridine nitrogen, one sulfur, and two ring oxygen donors remaining uncoordinated. The cadmium(II) coordination in **2** can be described as a distorted octahedral geometry, where S1, N2, S3, and N4 atoms from each macrocycle form the square plane, while two nitrato oxygens (O8 and O5) occupy the axial positions [O8–Cd1–O5 164.52(16)°]. Each monodentate nitrato group is bonded asymmetrically to the cadmium(II) with bond lengths [Cd1–O5 2.364(4), Cd1–O8 2.415(5) Å] that fall within the range observed for other monodentate nitrate complexes of the cadmium(II).[9] The Cd–S bond lengths [Cd1–S1 2.726(1), Cd1–S3 2.725(1) Å] are typical.[10c,11]

Recently, we have reported three Cd(II) complexes of 1,10-dithia-18-crown-6 (DT18C6) with different anions (ClO_4^-, NO_3^-, and I^-) which commonly show an endocyclic mononuclear structure, adopting a tight-and-bent conformation. These results suggest that the cavity size of the 18-membered ring is larger compared to that of Cd(II). Thus, the formation of the exocyclic complex **2** can be explained because of the anion coordination together with the larger cavity size of L^1 compared to that of Cd(II).

Anion-Dependent Nickel(II) Complexes of L^1 (3 and 4). Thiaaza-macrocycles are also suited to binding transition metal ions. So, nickel(II) salts with different anions (ClO_4^- and NO_3^-) were employed in the reactions with L^1, and then the anion-dependent products **3** and **4** with different stoichiometries and nickel(II) positions in the complexes were obtained, respectively, as depicted in Scheme 2.

The complexations of L^1 with $Ni(ClO_4)_2{\cdot}6H_2O$ and $Ni(NO_3)_2{\cdot}6H_2O$ afforded one violet 1:1 (metal-to-ligand) complex $[Ni(L^1)(CH_3CN)_3](ClO_4)_2{\cdot}2CH_3CN$ (**3**) (Figure 2a) and one sky blue 1:2 complex $[Ni(L^1)_2(NO_3)_2]$ (**4**) (Figure 2b),

dx.doi.org/10.1021/ic400247q | Inorg. Chem. 2013, 52, 8416–8426

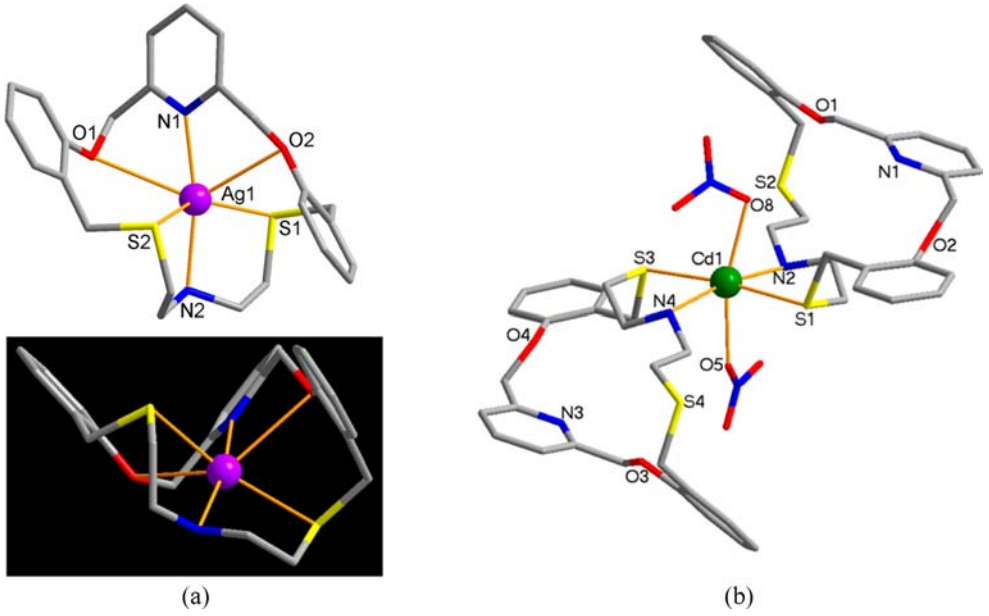

Figure 1. Crystal structures of (a) the endocyclic 1:1 (metal-to-ligand) complex **1**, $[Ag(\mathbf{L}^1)]NO_3$ (top: front view and bottom: side view) and (b) the exocyclic 1:2 complex **2**, $[Cd(\mathbf{L}^1)_2(NO_3)_2]$. Noncoordinating anion is omitted.

Table 1. Selected Bond Distances (Å) and Bond Angles (deg) for 1 and 2

Complex **1**			
Ag1−N1	2.342(2)	Ag1−N2	2.419(2)
Ag1−S1	2.648(1)	Ag1−S2	2.642(1)
Ag1−O1	2.952(2)	Ag1−O2	2.904(2)
N1−Ag1−N2	168.65(6)	N1−Ag1−S2	95.74(4)
N2−Ag1−S2	80.35(5)	N1−Ag1−S1	109.16(4)
N2−Ag1−S1	79.34(5)	S2−Ag1−S1	143.90(2)
N1−Ag1−O2	65.46(5)	N2−Ag1−O2	125.42(5)
S2−Ag1−O2	96.99(3)	S1−Ag1−O2	71.69(3)
N1−Ag1−O1	62.08(5)	N2−Ag1−O1	106.60(6)
S2−Ag1−O1	78.33(3)	S1−Ag1−O1	136.30(3)
O2−Ag1−O1	126.41(4)		
Complex **2**			
Cd1−N2	2.321(4)	Cd1−N4	2.329(4)
Cd1−S1	2.726(1)	Cd1−S3	2.725(1)
Cd1−O5	2.364(4)	Cd1−O8	2.415(5)
N2−Cd1−N4	169.32(13)	N2−Cd1−O5	89.87(14)
N4−Cd1−O5	79.46(13)	N2−Cd1−O8	79.57(14)
N4−Cd1−O8	110.74(14)	O5−Cd1−O8	164.52(16)
N2−Cd1−S3	100.26(9)	N4−Cd1−S3	80.78(9)
O5−Cd1−S3	91.35(13)	O8−Cd1−S3	101.59(12)
N2−Cd1−S1	80.83(9)	N4−Cd1−S1	97.02(9)
O5−Cd1−S1	82.55(13)	O8−Cd1−S1	84.59(12)
S3−Cd1−S1	173.82(4)		

respectively. The crystal structures are shown in Figure 2, and selected geometric parameters are presented in Table 2.

In **3**, the Ni(II) center is six-coordinate, being bound facially to NS_2 donors of $\mathbf{L}^1$ with one pyridine nitrogen and two ring oxygen donors remaining uncoordinated because of the relatively small ionic size of the Ni(II). The coordination sphere in **3** is completed by three acetonitrile solvent molecules which are located on the one side of the bound macrocycle with the nickel(II) positioned 1.433(1) Å from the NS_2 plane toward the solvato-ligands, adopting a perching conformation (Figure 2a). The nickel(II) coordination in **3** can be described as a distorted

Scheme 2. Anion-Dependent Endocyclic 1:1 (1) and Exocyclic 1:2 (2) Nickel(II) Complexes of L^1

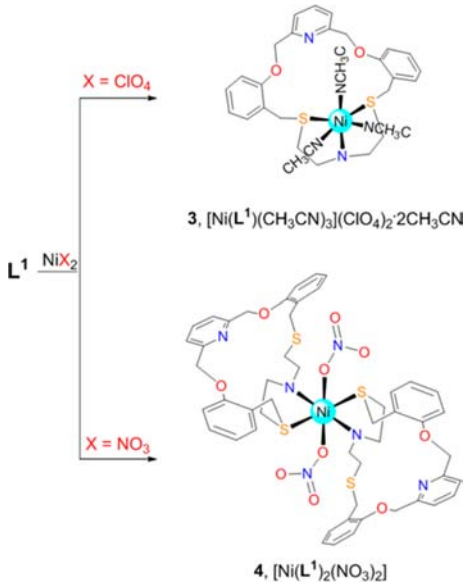

octahedral geometry, where S1, S2, N3, and N4 atoms form the square plane, while N2 and N5 atoms occupy the axial positions [N2−Ni1−N5 179.48(13)°]. The Ni−S bond lengths [Ni1−S1 2.392(1), Ni1−S2 2.435(1) Å] are typical.[12] The preference of the perching coordination mode in **3** may be due to the weaker affinity of ClO_4^- toward the metal ions which leads the anion to be excluded from the solvato-coordination sphere. As preliminary work for the ligand substitution by using the labile nature of the tris(CH_3CN) ligation in **3**, the treatment with KSCN gave the results that the CH_3CN peaks in the IR spectrum disappeared and, instead, the SCN^- peak appeared, suggesting the ligand substitution occurs (Figure S3 in Supporting Information).

In marked contrast to the Ni(II) position in **3**, the nitrato complex **4** shows an unusual 1:2 sandwich-like arrangement in which the exocyclic Ni(II) has a distorted octahedral environ-

dx.doi.org/10.1021/ic400247q | Inorg. Chem. 2013, 52, 8416−8426

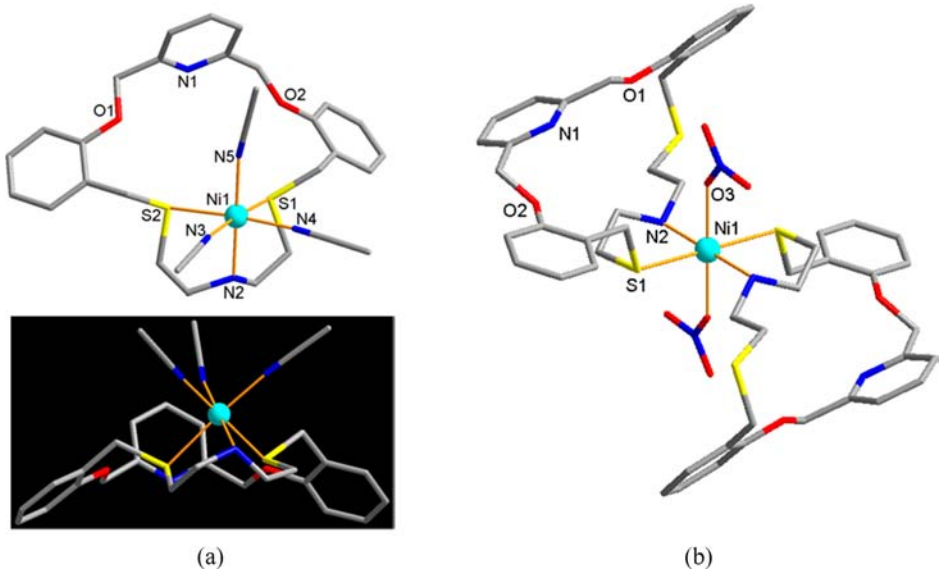

Figure 2. Crystal structures of (a) the endocyclic 1:1 (metal-to-ligand) complex **3**, $[Ni(\mathbf{L}^1)(CH_3CN)_3](ClO_4)\cdot 2CH_3CN$ (top: front view and bottom: side view) and (b) the exocyclic 1:2 complex **4**, $[Ni(\mathbf{L}^1)_2(NO_3)_2]$. Noncoordinating anions and solvent molecules are omitted.

Table 2. Selected Bond Distances (Å) and Bond Angles (deg) for 3 and 4[a]

Complex **3**			
Ni1−N2	2.091(3)	Ni1−N3	2.059(3)
Ni1−N4	2.064(3)	Ni1−N5	2.057(3)
Ni1−S1	2.392(1)	Ni1−S2	2.435(1)
Ni1···N1	5.529(3)		
N5−Ni1−N3	89.71(1)	N5−Ni1−N4	89.05(13)
N3−Ni1−N4	88.79(1)	N5−Ni1−N2	179.48(13)
N3−Ni1−N2	90.75(1)	N4−Ni1−N2	91.22(12)
N5−Ni1−S1	95.52(1)	N3−Ni1−S1	174.71(10)
N4−Ni1−S1	90.47(9)	N2−Ni1−S1	84.03(9)
N5−Ni1−S2	96.13(10)	N3−Ni1−S2	92.63(9)
N4−Ni1−S2	174.63(10)	N2−Ni1−S2	83.59(9)
S1−Ni1−S2	87.63(3)		
Complex **4**			
Ni1−N2	2.122(4)	Ni1−S1	2.439(1)
Ni1−O3	2.054(4)		
O3−Ni1−O3A	180.00(3)	O3−Ni1−N2A	83.08(19)
O3A−Ni1−N2A	96.92(19)	N2A−Ni1-N2	180.00(2)
O3−Ni1−S1	86.87(14)	O3A−Ni1−S1	93.13(14)
N2A−Ni1−S1	94.55(13)	N2−Ni1−S1	85.44(13)
S1−Ni1−S1A	180.00(4)		

[a]Symmetry operations: (A) $-x + 1, -y + 1, -z + 1$.

ment. Similar to the above cadmium(II) nitate complex **2** (Figure 1b), each macrocycle in **4** coordinates in a bidentate fasion via one sulfur and one secondary amine nitrogen. The coordination sphere is also completed by two monodentate nitrato ligands, with one pyridine nitrogen, one sulfur, and two oxygen donors in each $\mathbf{L}^1$ remaining uncoordinated. Again, the Ni(II) coordination in **4** can be described as a distorted octahedral geometry, where S1, S1A, N2, and N2A atoms form the square plane, while O3 and O3A atoms occupy the axial positions [O3−Ni1−O3A 180.00(3)°]. The Ni1−O(NO_3^-) bond lengths [2.054(4) Å] are comparable to those reported previously for such bonds.[12d] Accordingly, the strong binding of two NO_3^- toward the Ni atom inhibits the formation of the typical endotype structure and induces the unusual exotype SNO−Ni(II) coordination.

From these results for the Ni(II) complexes, it is concluded that the discriminated anion coordination ability alters the ligand behavior and has important consequences for the coordination mode and stoichiometry of the complexes. Previously, we observed the similar anion-dependent coordination modes for the Ag(I) and Hg(II) complex system.[8,13] Rodríguez-Blas group has reported the counterion-dependent endo-/exocoordinated Zn complexes of the diazacrown derivatives.[14] As far as we are aware, our results are the first example which gives the coordination mode and stochiometry change together upon changing the anions in the sulfur-containing macrocyclic complex system. Consequently, we can further generalize the fact that the anion coordination ability can be one of the important factors that controls not only the metal ion position but also their complex stoichiometry together, at least, in the thiamacrocyclic coordination system.

Dinuclear Silver(I) Complexes of $\mathbf{L}^2$ (5−7). Having obtained several different types of mononuclear complexes of $\mathbf{L}^1$ depending on the metal cations or anions, we proceeded to the preparation of dinuclear complexes of the larger macrocycle $\mathbf{L}^2$ with the extended structures as depicted in Scheme 3. The treatment of $\mathbf{L}^2$ with $AgNO_3$ resulted in the formation of two disilver(I) complexes **5** and **6** with different coordination environments. Notably, the solvent-mediated rearrangement of **5** to **6** was observed, which is an example of the conversion from a *kinetic* (**5**) to a *thermodynamic* (**6**) controlled products. In acidic condition, a disilver(I) complex **7** adopting a stair-type 1-D polymeric structure linked by anions was isolated. Structures of the three disilver(I) complexes **5**−**7** were characterized by single crystal X-ray analysis (Figures 3 and 4).

The reaction of $\mathbf{L}^2$ with $AgNO_3$ in dichloromethane/acetonitrile at room temperature yielded initially (within several hours) very small amounts of (two or three crystals, below 2% yield) cube-shaped crystalline product **5**. Fortunately, we were able to obtain the single crystal structure of **5** that exhibits a solvato-type disilver(I) complex with the formula being $[Ag_2(\mathbf{L}^2)(CH_3CN)_2](NO_3)_2$. Then, after one week later in the same vial, a block-type crystalline complex $[Ag_2(\mathbf{L}^2)](NO_3)_2$ (**6**) was isolated in high yield (~70%). Phase puity of the final product **6** was confirmed by powder X-ray diffraction (PXRD)

dx.doi.org/10.1021/ic400247q | *Inorg. Chem.* 2013, 52, 8416−8426

Scheme 3. Disilver(I) Complexes (5−7) of L^2 Showing Different Coordination Environments

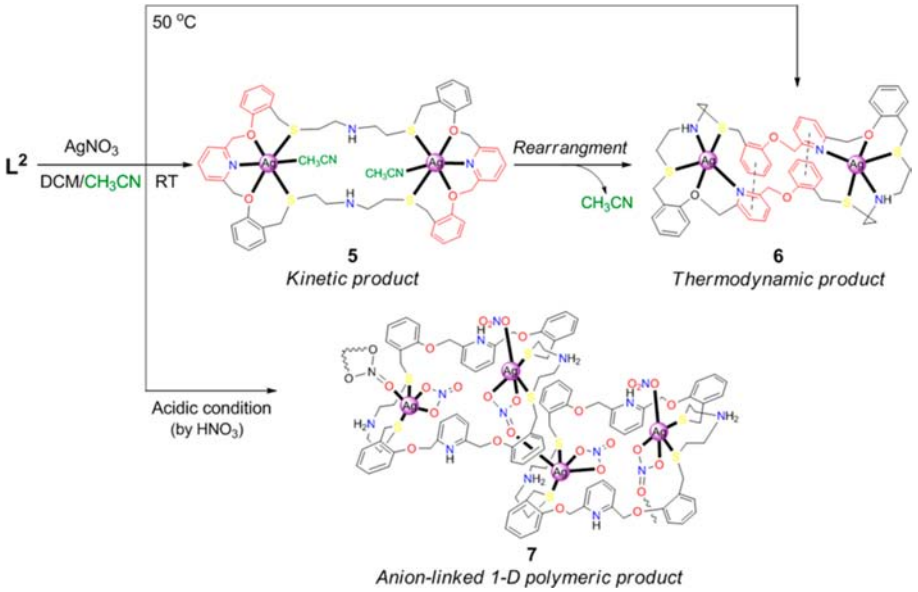

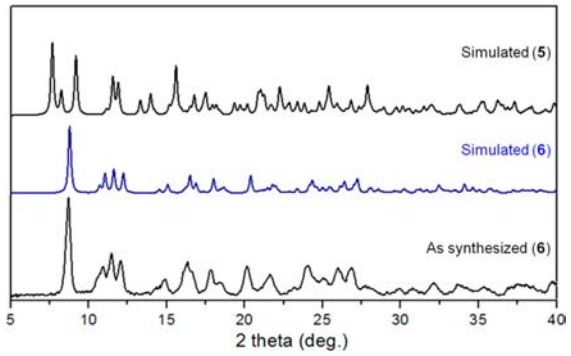

Figure 3. PXRD patterns of **5** and **6**: the experimental data for **5** are not available because of the extremely low yield.

(Figure 3), suggesting no further existence of **5**. Under the identical reaction condition but at 50 °C, only the complex **6** was obtained directly as dipected in Scheme 3. Because of this reason, we believe that the solvato-type disilver(I) complex **5** as the *kinetic* controlled product with a larger empty space inside the macrocyclic cavity transforms toward a more stable structured **6** as the *thermodynamic* controlled product.

As seen from Figure 4, one of the common strucutral features in **5** and **6** is that $\mathbf{L}^2$ possesses two silver(I) ions to form a $[Ag_2(\mathbf{L}^2)]^{2+}$ type discrete disilver(I) complex unit. X-ray analysis revealed that the gross geometry of the solvato-complex **5** is similar to the peanut shell structure (Figure 4a), and then the disilver(I) complex can be divided by the crosscut of two secondary amine N2 and N2A atoms. The selected geometric parameters of **5** are presented in Table 3. Since there is an inversion at the center of the molecule, the asymmetric unit of **5** in the complex part contains one Ag atom, a half molecule of the ligand, and one acetonitrile. The Ag(I) center is six-coordinate, being bound to one pyridine nitrogen, two oxygens, and two sulfur donors in one side of $\mathbf{L}^2$ with the macrocycle adopting a "twisted" conformation. The remaining coordination sites are occupied by one acetonitrile molecule. Thus, the coordination sphere of the Ag(I) center is a distorted pentagonal pyramid. The bite angles around the metal center vary considerably, ranging 66.1° (N1−Ag1−O2) to 91.4° (S1−Ag1−S2) due to the open space between two Ag atoms (Ag1···Ag1A 10.1 Å). Notably, two secondary nitrogen donors in the middle of $\mathbf{L}^2$ are not bound.

Next, the thermodynamic product **6** also adopts a disilver(I) complex (Figure 4b), but its coordination environment is quite different from that of **5**. The selected geometric parameters of **6** are presented in Table 4. Since there is an imposed inversion at the center of the molecule, its asymmetric unit contains one Ag atom and a half molecule of $\mathbf{L}^2$. Basically, the rearrangement of **5** to **6** is induced by the removal of the coordinated acetonitrile molecules in **5**. Thus, the Ag(I) center in **6** is five-coordinate, being bound to one pyridine nitrogen, one secondary nitrogen, two sulfurs, and one oxygen: the NO_2S_2 (in **5**) and N_2OS_2 (in **6**) donors coordinate to each metal center.

The solvato-complex **5** whose formation is initiated by the excess amount of solvent molecules with high coordinating ability (acetonitrile) seems to be less stable and converted to the more stable form **6**. In the rearrangement from **5** to **6**, the conformational change of the ligand is much more critical. For example, the pyridine-O1-benzene subunits locate at both ends of **5**, while the same subunits in **6** locate at the center of the molecule, showing the two sets of the face-to-face type $\pi-\pi$ stacking between pyridine and benzene rings (dashed lines in Figure 6b, centroid-to-centroid distance 3.941 Å). Since the Ag···Ag separation in **6** (7.3 Å) is much shorter than that in **5** (10.1 Å), the kinetic product **5** provides the larger empty cavity space than that of thermodynamic product **6**. At 50 °C, as shown in Scheme 3, only **6** was obtained. Consequently, the spontaneous rearragement of **5** to **6** may be understood to be entropically favorable.

After obtaining the two types of disilver(I) complexes of $\mathbf{L}^2$ in the neutral condition, we have carried out the same reaction in acidic and basic conditions. Initially, we were unable to obtain a meaningful crystalline complex of $\mathbf{L}^2$ in the basic condition. In the acidic condition (by adding HNO_3), a colorless crystalline product **7** with the formula being $\{[Ag_2(H_4\mathbf{L}^2)(\mu_2\text{-}NO_3)(NO_3)_2](NO_3)_3\cdot CH_3CN\cdot 3H_2O\}_n$ was isolated. The complex **7** is a disilver(I) complex, adopting a 1-D stairway-like polymeric species linked with nitrate ions (Figure 5). The selected geometric parameters of **7** are presented in Table 5. The

dx.doi.org/10.1021/ic400247q | *Inorg. Chem.* 2013, 52, 8416−8426

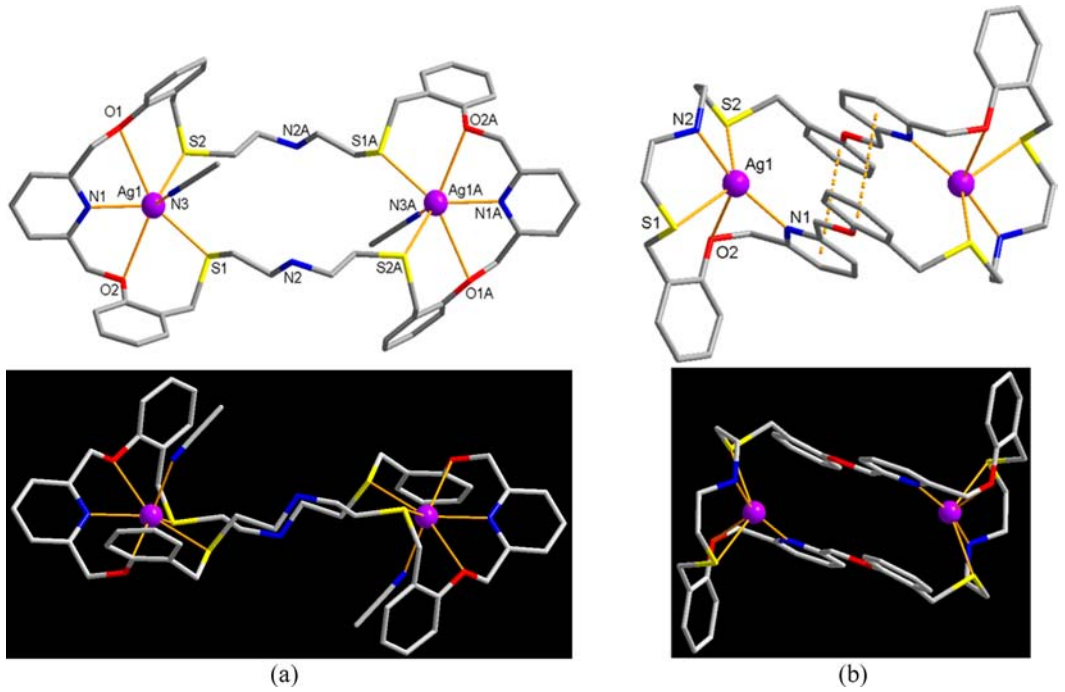

Figure 4. Crystal structures of (a) disilver(I) solvato-complex **5**, $[Ag_2(\mathbf{L}^2)(CH_3CN)_2](NO_3)_2$ and (b) solvent-free disilver(I) complex **6**, $[Ag2(\mathbf{L}^2)](NO_3)_2$: (top) general view and (bottom) side view. Noncoordinating anions are omitted.

Table 3. Selected Bond Distances (Å) and Bond Angles (deg) for 5[a]

Ag1−N1	2.331(7)	Ag1−N3	2.426(9)
Ag1−S1	2.618(2)	Ag1−S2	2.631(2)
Ag1−O1	2.892(6)	Ag1−O2	2.809(5)
Ag1···Ag1A	10.128(2)		
N1−Ag1−N3	104.00(3)	N1−Ag1−S1	138.51(18)
N3−Ag1−S1	90.79(19)	N1−Ag1−S2	117.03(15)
N3−Ag1−S2	111.9(2)	S1−Ag1−S2	91.49(7)
N1−Ag1−O2	66.10(2)	N3−Ag1−O2	119.70(2)
S1−Ag1−O2	72.84(13)	S2−Ag1−O2	125.73(13)
N1−Ag1−O1	66.20(2)	N3−Ag1−O1	77.70(2)
S1−Ag1−O1	155.19(13)	S2−Ag1−O1	73.12(12)
O2−Ag1−O1	131.94(16)		

[a]Symmetry operations: (A) $-x, -y, -z + 1$.

Table 4. Selected Bond Distances (Å) and Bond Angles (deg) for 6[a]

Ag1−N1	2.259(4)	Ag1−N2	2.367(5)
Ag1−S1	2.714(2)	Ag1−S2	2.708(2)
Ag1−O2	2.825(4)	Ag1···Ag1A	7.309(1)
N1−Ag1−N2	163.90(17)	N1−Ag1−S2	108.10(11)
N2−Ag1−S2	76.87(13)	N1−Ag1−S1	109.15(11)
N2−Ag1−S1	77.21(13)	S2−Ag1−S1	128.22(5)
N1−Ag1−O2	66.47(14)	N2−Ag1−O2	129.62(14)
S2−Ag1−O2	82.83(9)	S1−Ag1−O2	80.46(9)

[a]Symmetry operations: (A) $-x + 2, -y, -z + 2$.

asymmetric unit of the complex part of **7** contains one $\mathbf{L}^2$, two Ag atoms, and three nitrate ions.

Both of Ag(I) centers (Ag1 and Ag2) in **7** that lie inside the macrocyclic cavity are five-coordinate. One part of the macrocycle coordinates to each Ag(I) ion in a bidentate fashion via S_2 donors, and the coordination environment is completed by one bridging bidentate nitrate ion and one terminal monodentate nitrate ion. Notably, these disilver(I) complex units are linked by one nitrato ligand via Ag1-(μ_2-NO_3)−Ag2A bonds, adopting a 1-D polymeric array with a "stairway" conformation (Figure 5c). The Ag1···Ag2 separation in the large cavity is 9.054(1) Å and that in the Ag1-(μ_2-NO_3)−Ag2A between two cavities is 5.233(1) Å. The pyridine nitrogen and the secondary amine nitrogen atoms which are protonated remain uncoordinated. In **7**, the bond distances of Ag−S (thioether) [2.504(2)−2.544(2) Å] are typical.[9] Overall, it seems that the protonated nitrogen donors and the coordination of nitrate ions toward the metal center in the presence of HNO_3 provide the stabilization of the observed unique dinuclear 1-D networking behavior of the large macrocycle.

NMR Titration and ESI-Mass Studies of Silver(I) Complexation in Solution. As mentioned above, the mononuclear and dinuclear Ag(I) complexes of $\mathbf{L}^1$ and $\mathbf{L}^2$ have been isolated in the solid state and structurally characterized by the single crystal X-ray analysis, respectively. In order to explore the complexation behaviors in solution and also for comparison with the solid state behaviors observed, ^{1}H NMR titration and ESI mass experiments for each Ag(I) complex system were performed in the solution state (Figures 6−8; see complete NMR spectra in Supporting Information).

In the NMR titrations, the signals of the methylene protons ($H_{1\text{-}4}$) and the aromatic protons ($H_{a\text{-}f}$) for each macrocycle are well resolved and readily identified except for the signal of the H_3 proton in $\mathbf{L}^2$ because of the overlapping with the solvent peak (Figures 6a and 7a). The chemical shift changes ($\Delta\delta$, ppm) of each peak was measured as a function of the mole ratio of Ag(I) to ligand ($Ag^+/\mathbf{L}^1$) (Figures 6b and 7b). Upon stepwise addition of $AgNO_3$ (0−1.6 equiv for $\mathbf{L}^1$ and 0−2.8 equiv for $\mathbf{L}^2$) to each ligand solution, the signals for all protons shifted downfield (or upfield in some cases), in keeping with the occurrence of the Ag(I) complex formation, with the ligand exchange rate being fast on the NMR time scale (300 MHz).

dx.doi.org/10.1021/ic400247q | Inorg. Chem. 2013, 52, 8416−8426

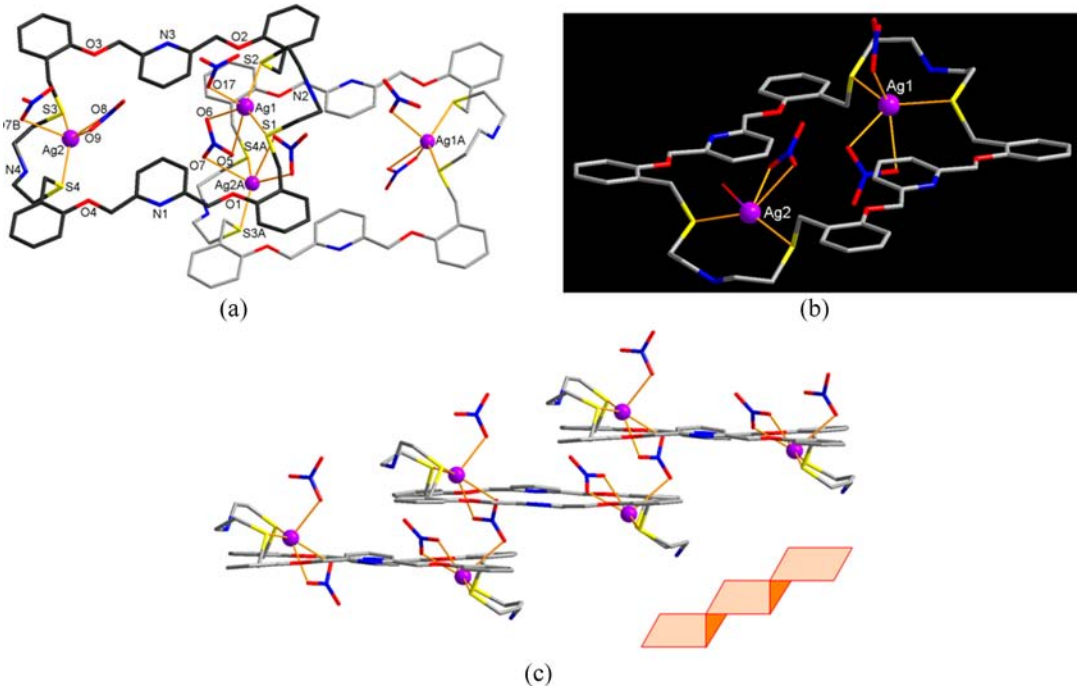

Figure 5. Crystal structure of **7**, $\{[Ag_2(H_4L^2)(\mu_2\text{-}NO_3)(NO_3)_2](NO_3)_3\cdot CH_3CN\cdot 3H_2O\}_n$; (a) basic coordination environment, (b) general view of one macrocyclic disilver(I) complex unit, and (c) side view of a stairlike 1-D polymeric chain linked with one nitrate ion. Noncoordinating solvent molecules are omitted.

Table 5. Selected Bond Distances (Å) and Bond Angles (deg) for 7[a]

Ag1−S1	2.544(2)	Ag1−S2	2.530(2)
Ag2−S3	2.504(2)	Ag2−S4	2.536(2)
Ag1−O5	2.644(6)	Ag1−O6	2.479(7)
Ag1−O17	2.515(7)	Ag2−O7A	2.823(9)
Ag2−O8	2.483(6)	Ag2−O9	2.620(6)
Ag1···Ag2	9.054(1)	Ag1···Ag2A	5.233(1)
O6−Ag1−O17	85.90(3)	O6−Ag1−S2	99.39(17)
O17−Ag1−S2	98.92(19)	O6−Ag1−S1	128.86(16)
O17−Ag1−S1	94.80(2)	S2−Ag1−S1	130.63(6)
O6−Ag1−O5	49.13(18)	O17−Ag1−O5	114.50(2)
S2−Ag1−O5	128.59(15)	S1−Ag1−O5	85.85(13)
O8−Ag2−S3	96.70(15)	O8−Ag2−S4	119.23(17)
S3−Ag2−S4	139.04(6)	O8−Ag2−O9	48.79(18)
S3−Ag2−O9	139.16(14)	S4−Ag2−O9	81.80(14)
O8−Ag2−O7A	110.82(19)	S3−Ag2−O7A	95.03(13)
S4−Ag2−O7A	90.11(13)	O9−Ag2−O7A	81.70(2)

[a]Symmetry operations: (A) $x + 0.5, -y + 0.5, z + 0.5$.

In the case of $\mathbf{L}^1$, the titration curves (Figure 6b) show that the plots for all proton signals exhibit no more cation-induced shifts above a mole ratio ($Ag^+/\mathbf{L}^1$) of 1.0, indicating a 1:1 (metal-to-ligand) stoichiometry for the complex, which is identical to that observed in the solid state (Figure 1a). Notably, the observed larger downfield shifts for the aliphatic proton (H_4) adjacent to the secondary amine N atom are in accord with the Ag(I) being strongly bound to the N donor in the solid state shown in complex **1**. The larger downfield shifts of the pyridyl protons (H_a and H_b) also show the contribution of the hetero N atom to the coordination.

Meanwhile, the titration curves for $\mathbf{L}^2$ show inflection points at a mole ratio ($Ag^+/\mathbf{L}^2$) of 1.0, indicating the initial formation of a 1:1 complex which is then converted into a 2:1 species as the concentration of Ag(I) increases (Figure 7b). The chemical shifts beyond the mole ratio of 2.0 are nearly constant, which suggest that the stable 2:1 complex is formed. Again, the larger downfield shifts of the pyridyl protons (H_a and H_b) also show the contribution of the hetero N atom to the coordination. Unlike $\mathbf{L}^1$, the directions of the chemical shift changes for the aliphatic protons ($H_{1,2,4}$) and the aromatic protons ($H_{c\text{-}f}$) in $\mathbf{L}^2$ are switched before and after the mole ratio of 1.0, perhaps reflecting the conformational rearrangement of the flexible macrocycle $\mathbf{L}^2$ upon stepwise dinuclear complexation and the presence of a related $\pi-\pi$ stacking interaction of the type observed in the solid structure of **6** (dashed lines in Figure 4b). Consequently, the NMR data suggest that the solution structures of the respective Ag(I) complexes with $\mathbf{L}^1$ and $\mathbf{L}^2$ are in general agreement with those occurring in the solid state.

The complexation behaviors of the macrocycles toward Ag(I) were further investigated by the ESI mass technique (Figure 8). The observed 1:1 stoichiometry for the complexation of $\mathbf{L}^1$ with Ag(I) was confirmed, which corresponds to the species $[Ag(\mathbf{L}^1)]^+$ (m/z 561.2, Figure 8a). The observed 2:1 stoichiometry for the complexation of $\mathbf{L}^2$ with Ag(I) is also confirmed by the corresponding complex solution, which corresponds to the species $[Ag_2(\mathbf{L}^2)]^{2+}$ (m/z 560.3, Figure 8b). These peaks are also verified by comparison of the relative abundance of their isotope peak patterns between observed peaks and the corresponding theoretical simulation. Again, it is noted that the behaviors of the proposed macrocycles in solution are in general agreement with those occurring in the solid state.

CONCLUSION

The 1:1 and 2:2 cyclization products with 20-membered ($\mathbf{L}^1$) and 40-membered ($\mathbf{L}^2$) ring cavities were employed, and their supramolecular complexes were prepared and structurally characterized. The crystal structures cover a range of structural types and coordination modes including mono- to dinuclear,

dx.doi.org/10.1021/ic400247q | Inorg. Chem. 2013, 52, 8416−8426

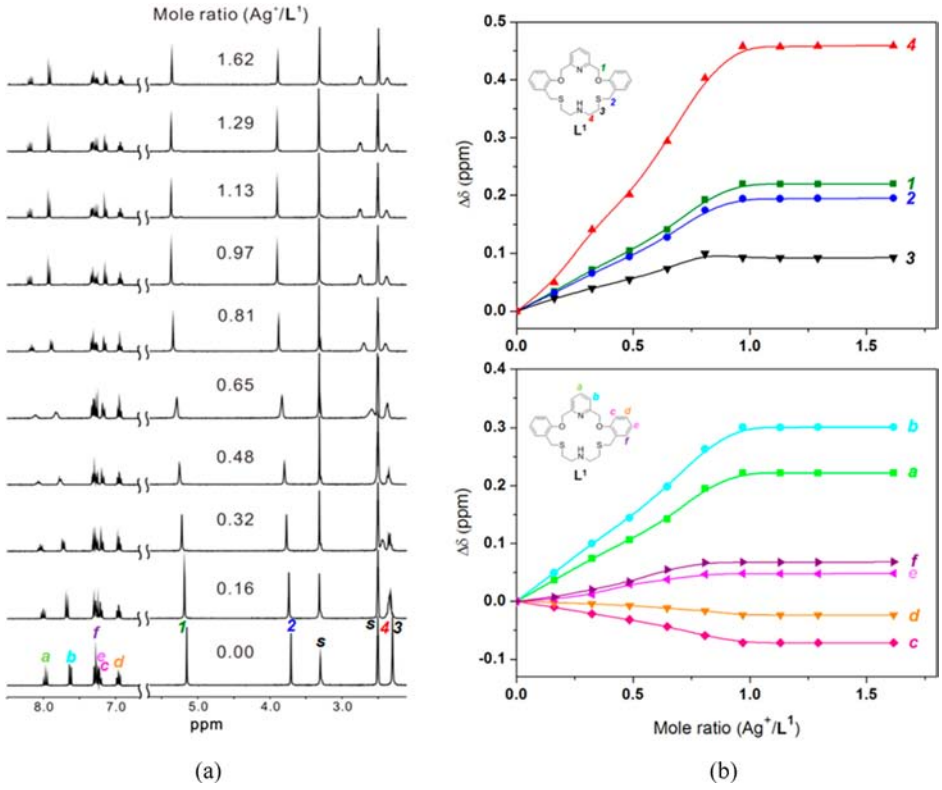

Figure 6. (a) The ^{1}H NMR spectra of $\mathbf{L^1}$ following the stepwise addition of $AgNO_3$ in DMSO-d_6 and (b) titration curves for $\mathbf{L^1}$ with $AgNO_3$: (top) aliphatic region and (bottom) aromatic region.

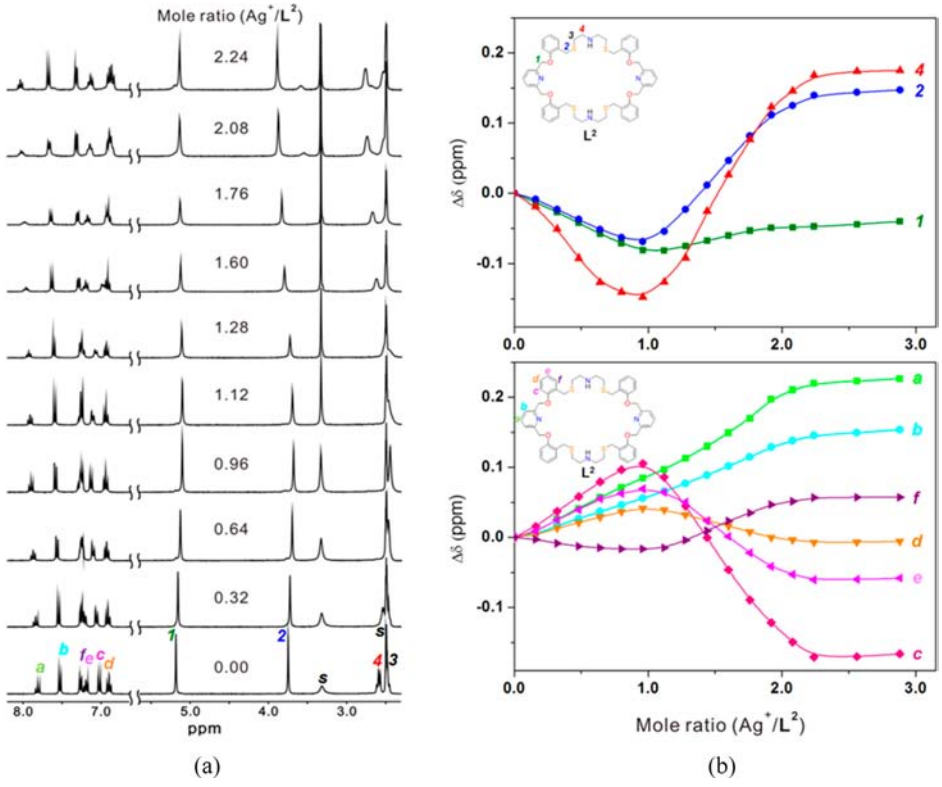

Figure 7. (a) The ^{1}H NMR spectra of $\mathbf{L^2}$ following the stepwise addition of $AgNO_3$ in DMSO-d_6 and (b) titration curves for $\mathbf{L^1}$ with $AgNO_3$: (top) aliphatic region and (bottom) aromatic region.

endo- to exocyclic, and discrete to continuous ones. Similar to the solid state structures, the formations of the mono- and disilver(I) complexes with the smaller and larger macrocyclic ligands in solution were confirmed by NMR titration and ESI

dx.doi.org/10.1021/ic400247q | Inorg. Chem. 2013, 52, 8416−8426

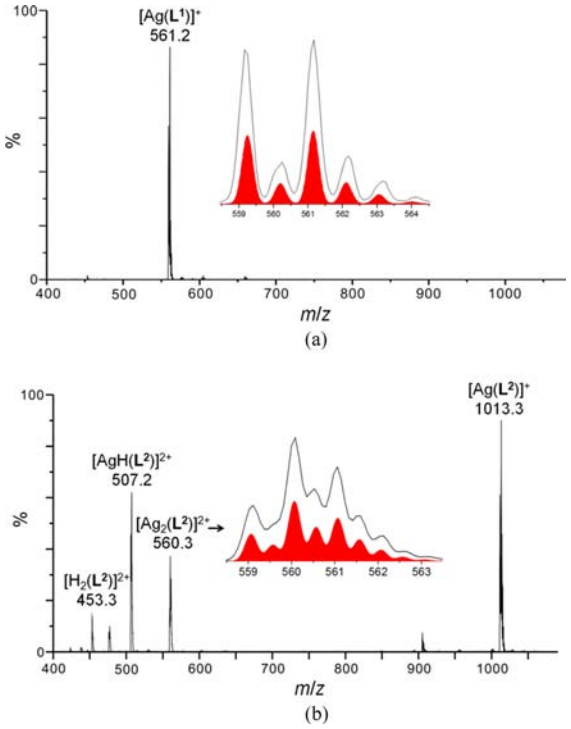

Figure 8. ESI-MS spectra of (a) $\mathbf{L^1}$ and (b) $\mathbf{L^2}$ in the presence of $AgNO_3$ (1.0 equiv for $\mathbf{L^1}$ and 2.0 equiv for $\mathbf{L^2}$) in acetonitrile. In each isotope pattern, the lower part (red) represents the predicted mass spectrum distribution for the ion.

mass studies. Since the larger macrocycle represents the potential to provide a wide range of binding properties, investigations aimed not only to obtain new types of binuclear species but also to prepare metallo-supramolecular network species are in progress.

EXPERIMENTAL SECTION

General. All chemicals and solvents used in the syntheses were reagent grade and were used without further purification. NMR spectra were recorded on a Bruker 300 spectrometer (300 MHz). The FT-IR spectra were measured with a Nicolet *i*S 10 spectrometer. The electrospray ionization (ESI) mass spectra were obtained on a Thermo Scientific LCQ Fleet spectrometer. The elemental analysis was carried out on a LECO CHNS-932 elemental analyzer. The PXRD patterns were recorded on a Bruker D8 Discover with GADDS.

Caution! *Perchlorate salts of metal complexes are potentially explosive and should be handled with great care.*

Preparation of 1, $[Ag(L^1)]NO_3$. A solution of $AgNO_3$ (9.2 mg, 0.0542 mmol) in acetonitrile (2 mL) was added to a solution of $\mathbf{L^1}$ (20.1 mg, 0.0444 mmol) in dichloromethane (2 mL). Slow evaporation of the solution afforded a colorless crystalline product **1** suitable for X-ray analysis. Yield (50%); Mp: 187−188 °C (decomp.). IR (KBr, cm^{-1}): 3471, 3062, 2945, 2839, 1598, 1492, 1455, 1381 (NO_3^-), 1357, 1241, 1106, 1032, 771, 754. Anal. calcd. for $C_{25}H_{28}AgN_3S_2O_5$ (%): C, 48.24; H, 4.53; N, 6.75; S, 10.30. Found: C, 48.64; H, 4.55; N, 6.58; S, 10.45. Mass spectrum *m*/*z* (ESI): 561.25 for $[Ag(L^1)]^+$ (calcd 561.06).

Preparation of 2, $[Cd(L^1)_2(NO_3)_2]$. A solution of $Cd(NO_3)_2{\cdot}4H_2O$ (15.1 mg, 0.0491) in acetonitrile (2 mL) was added to a solution of $\mathbf{L^1}$ (20.2 mg, 0.0446 mmol) in dichloromethane (2 mL). Slow evaporation of the solution afforded a colorless crystalline product **2** suitable for X-ray analysis. Yield (30%); Mp: 224−226 °C. IR (KBr, cm^{-1}): 3475, 3033, 2933, 2863, 1654, 1595, 1493, 1452, 1384 (NO_3^-), 1365, 1292, 1243, 1104, 1043, 1015, 941, 753. Anal. calcd. for $C_{50}H_{56}CdN_6S_4O_{10}$ (%): C, 52.60; H, 4.94; N, 7.36; S, 11.23. Found: C, 52.40; H, 5.10; N, 7.70; S, 10.89. Mass spectrum *m*/*z* (ESI): 627.83 for $[Cd(L^1)NO_3]^+$ (calcd 628.05).

Preparation of 3, $[Ni(L^1)(CH_3CN)_3](ClO_4)_2{\cdot}2CH_3CN$. A solution of $Ni(ClO_4)_2{\cdot}6H_2O$ (12.5 mg, 0.0493 mmol) in acetonitrile (2 mL) was added to a solution of $\mathbf{L^1}$ (20.1 mg, 0.0444 mmol) in dichloromethane (2 mL). Slow evaporation of the solution afforded a violet crystalline product **3** suitable for X-ray analysis. Yield (45%); Mp: 225−227 °C (decomp.). IR (KBr, cm^{-1}): 3405, 3219, 2359, 2341, 1608, 1492, 1453, 1243, 1180, 1089 (ClO_4^-), 994, 792, 765, 624. Anal. calcd for $C_{35}H_{43}NiN_7S_2O_{10}Cl_2$ (%): C, 45.92; H, 4.73; N, 10.71; S, 7.00. Found: C, 45.61; H, 4.56; N, 10.15; S, 6.78. Mass spectrum *m*/*z* (ESI): 608.75 for $[Ni(L^1)ClO_4]^+$ (calcd 609.04).

Preparation of 4, $[Ni(L^1)_2](NO_3)_2$. A solution of $Ni(NO_3)_2{\cdot}6H_2O$ (14.4 mg, 0.0495 mmol) in acetonitrile (2 mL) was added to a solution of $\mathbf{L^1}$ (20.4 mg, 0.0450 mmol) in dichloromethane (2 mL). Slow evaporation of the solution afforded a sky blue crystalline product **4** suitable for X-ray analysis. Yield (15%); Mp: 178−180 °C (decomp.). IR (KBr, cm^{-1}): 3356, 3062, 2932, 2873, 2737, 1598, 1492, 1454, 1384 (NO_3^-), 1294, 1241, 1180, 1101, 1041, 995, 760. Anal. calcd for $C_{50}H_{56}NiN_6S_4O_{10}$ (%): C, 55.20; H, 5.19; N, 7.72; S, 11.79. Found: C, 55.10; H, 5.61; N, 7.91; S, 12.00. Mass spectrum *m*/*z* (ESI): 255.17 for $[Ni(L^1)]^{2+}$ (calcd 255.05) and 571.75 for $[Ni(L^1)NO_3]^+$ (calcd 572.08).

Preparation of 5, $[Ag_2(L^2)(CH_3CN)_2](NO_3)_2$ and 6, $[Ag_2(L^2)](NO_3)_2$. A solution of $AgNO_3$ (8.3 mg, 0.0489 mmol) in acetonitrile (2 mL) was added to a solution of $\mathbf{L^2}$ (20.1 mg, 0.0222 mmol) dichloromethane (2 mL). Slow evaporation of the solution afforded two kinds of crystals: at the beginning (within 3 h) tiny cube-type crystals of **5** (two or three crystals, below 2% yield) formed on the wall of the vial, which converted to the block-shaped crystals of **6** (70% yield) after one week. One crystal of **5** was isolated carefully from the mother liquor for the X-ray crystallographic measurements. The molecular formula of **5** was established on the basis of X-ray analysis. The final product was collected by filtration and washed with acetonitrile and diethyl ether, and dried under reduced pressure. The PXRD measurements as well as analytical results (elemental analysis and IR) excluded the presence of **5** in the final product. Separately, another reaction mixture of $\mathbf{L^2}$ and $AgNO_3$ in acetonitrile/dichloromethane was heated at 50 °C for 10 min. The resulting solution was allowed to stand at room temperature, yielding colorless block-shaped crystals of **6**. For **6**: yield (70%); Mp: 194−195 °C (decomp.). IR (KBr, cm^{-1}): 3482, 3224, 3065, 2930, 2845, 1600, 1493, 1455, 1384 (NO_3^-), 1244, 1105, 1052, 1015, 753. Anal. calcd. for $C_{50}H_{56}Ag_2N_6S_4O_{10}$ (%): C, 48.24; H, 4.53; N, 6.75; S, 10.30. Found: C, 48.97; H, 4.56; N, 6.46; S, 10.18. Mass spectrum *m*/*z* (ESI): 560.33 for $[Ag_2(L^2)]^{2+}$ (calcd 560.06) and 1181.83 for $[Ag_2(L^2)NO_3]^+$ (calcd 1182.12).

Preparation of 7, $\{[Ag_2(H_4L^2)(\mu_2\text{-}NO_3)(NO_3)_2](NO_3)_3{\cdot}CH_3CN{\cdot}3H_2O\}_n$. A solution of $AgNO_3$ (8.3 mg, 0.0489 mmol) in acetonitrile (2 mL) was added to a solution of $\mathbf{L^2}$ (20.1 mg, 0.0222 mmol) in dichloromethane (2 mL). To acidify the reaction mixture, 1 mL of 1 M nitric acid was added. Slow evaporation of the solution afforded a colorless crystalline **7** suitable for X-ray analysis. Yield (50%); Mp: 144−145 °C. IR (KBr, cm^{-1}): 3493, 3064, 2763, 2602, 2400, 1658, 1623, 1599, 1587, 1494, 1454, 1384 (NO_3^-), 1301, 1245, 1188, 1166, 1113, 1037, 759. Anal. calcd for $C_{52}H_{69}Ag_2N_{11}S_4O_{25}$ (%): C, 39.23; H, 4.37; N, 9.68; S, 8.05. Found: C, 39.46; H, 4.16; N, 9.40; S, 7.89.

X-ray Crystallographic Analysis. Crystal data for **1**−**7** were collected on a Bruker SMART APEX II ULTRA diffractometer equipped with graphite monochromated Mo Kα radiation (λ = 0.71073 Å) generated by a rotating anode. The cell parameters for the compounds were obtained from a least-squares refinement of the spot (from 36 collected frames). Data collection, data reduction, and semiempirical absorption correction were carried out using the software package of APEX2.[15] All of the calculations for the structure determination were carried out using the SHELXTL package.[16] In all cases, all non-hydrogen atoms were refined anisotropically, and all hydrogen atoms except coordinated water molecules were placed in idealized positions and refined isotropically in a riding manner along with the their respective parent atoms. In the cases of coordinated water molecules, the initial positions of the hydrogen atoms were obtained from difference electron density maps and refined with riding constraints. Relevant crystal data collection and refinement data for the crystal structures of **1**−**7** are summarized in Table 6.

dx.doi.org/10.1021/ic400247q | *Inorg. Chem.* 2013, 52, 8416−8426

Table 6. Crystal and Experimental Data for 1−7

	1	2	3	4
formula	$C_{25}H_{28}AgN_3O_5S_2$	$C_{50}H_{54}CdN_6O_{10}S_4$	$C_{35}H_{43}Cl_2N_7NiO_{10}S_2$	$C_{50}H_{56}N_6NiO_{10}S_4$
formula weight	622.49	1139.63	915.49	1087.96
temperature (K)	173(2)	173(2)	173(2)	173(2)
crystal system	triclinic	triclinic	monoclinic	monoclinic
space group	$P\bar{1}$	$P\bar{1}$	$P2_1/c$	$P2_1/n$
Z	2	2	4	2
a (Å)	7.7858(2)	13.3879(2)	11.7296(2)	10.6383(13)
b (Å)	11.9975(3)	15.2353(3)	24.3066(4)	11.9057(14)
c (Å)	13.7046(3)	15.5975(3)	14.7652(2)	19.717(2)
α (°)	99.845(1)	115.3600(10)	90	90
β (°)	91.251(1)	90.3050(10)	97.654(1)	96.529(3)
γ (°)	99.378(1)	115.7620(10)	90	90
V (Å^3)	1242.81(5)	2516.40(8)	4172.15(11)	2481.1(5)
D_x (g/cm^3)	1.663	1.504	1.457	1.456
$2\theta_{max}$ (°)	52.00	52.00	52.00	52.00
R_1, wR_2 [$I > 2\sigma(I)$]	0.0256, 0.0593	0.0567, 0.1286	0.0513, 0.1120	0.0771, 0.1971
R_1, wR_2 [all data]	0.0312, 0.0620	0.0864, 0.1462	0.0900, 0.1307	0.1361, 0.2339
GOF	1.041	1.037	1.017	1.037
no. reflns used [$>2\sigma(I)$]	4894 [R_{int} = 0.0328]	9900 [R_{int} = 0.0508]	8200 [R_{int} = 0.0705]	4871 [R_{int} = 0.0952]
structure determination	SHELXTL	SHELXTL	SHELXTL	SHELXTL
refinement	full-matrix	full-matrix	full-matrix	full-matrix

	5	6	7
formula	$C_{50}H_{56}Ag_2N_6O_{10}S_4$	$C_{54}H_{62}Ag_2N_{10}O_{16}S_4$	$C_{52}H_{69}Ag_2N_{11}O_{25}S_4$
formula weight	1244.99	1451.12	1592.16
temperature (K)	173(2)	173(2)	173(2)
crystal system	monoclinic	monoclinic	monoclinic
space group	$P2_1/n$	$P2_1/n$	Cc
Z	2	2	4
a (Å)	8.4912(3)	13.3239(12)	21.1368(3)
b (Å)	14.4837(5)	10.9478(10)	25.1483(3)
c (Å)	20.2029(6)	20.3601(18)	14.0307(2)
α (°)	90	90	90
β (°)	93.951(2)	94.546(5)	121.866(1)
γ (°)	90	90	90
V (Å^3)	2478.73(14)	2960.5(5)	6334.04(15)
D_x (g/cm^3)	1.668	1.628	1.670
$2\theta_{max}$ (°)	52.00	48.00	52.00
R_1, wR_2 [$I > 2\sigma(I)$]	0.0573, 0.1178	0.0604, 0.1022	0.0548, 0.1466
R_1, wR_2 [all data]	0.1274, 0.1437	0.1567, 0.1330	0.0610, 0.1537
GOF	1.004	0.970	1.032
no. reflns used [$>2\sigma(I)$]	4879 [R_{int} = 0.0895]	4552 [R_{int} = 0.1742]	10845 [R_{int} = 0.0300]
structure determination	SHELXTL	SHELXTL	SHELXTL
refinement	full-matrix	full-matrix	full-matrix

■ ASSOCIATED CONTENT

Supporting Information

Complete NMR titration data. This material is available free of charge via the Internet at http://pubs.acs.org. CCDC (922278−922284) contain the supplementary crystallographic data for this paper. These data can be obtained free of charge from The Cambridge Crystallographic Data Center via www.ccdc.cam.ac.uk/data_request/cif.

■ AUTHOR INFORMATION

Corresponding Author

*E-mail: sslee@gnu.ac.kr.

Notes

The authors declare no competing financial interest.

■ ACKNOWLEDGMENTS

This work was supported by WCU program (R32-20003) and NRF (2010-0022499, 2011-0011064, and 2012R1A4A1027750).

■ REFERENCES

(1) (a) Pilkington, N. H.; Robson, R. *Aust. J. Chem.* **1970**, *23*, 2225. (b) Alberts, A. H.; Lehn, J.-M.; Parker, D. *J. Chem. Soc., Dalton Trans.* **1985**, 2311. (c) Menif, R.; Martell, A. E.; Squattrito, P. J.; Clearfield, A. *Inorg. Chem.* **1990**, *29*, 4723. (d) MacLachlan, M. J.; Park, M. K.; Thompson, L. K. *Inorg. Chem.* **1996**, *35*, 5492. (e) Brooker, S. *Coord. Chem. Rev.* **2001**, *222*, 33. (f) de Geest, D. J.; Noble, A.; Moubaraki, B.; Murray, K. S.; Larsen, D. S.; Brooker, S. *Dalton Trans.* **2007**, 467. (g) Cameron, S. A.; Brooker, S. *Inorg. Chem.* **2011**, *50*, 3697.

(2) (a) Kim, H.-S.; Kwon, I.-C.; Choi, J.-H. *J. Heterocycl. Chem.* **1999**, *36*, 1285. (b) Habata, Y.; Seo, J.; Otawa, S.; Osaka, F.; Noto, K.; Lee, S. S. *Dalton Trans.* **2006**, 2202.

(3) Jung, D.; Chamura, R.; Habata, Y.; Lee, S. S. *Inorg. Chem.* **2011**, *50*, 8392.
(4) Lindoy, L. F.; Meehan, G. V.; Vasilescu, I. M.; Kim, H. J.; Lee, J.-E.; Lee, S. S. *Coord. Chem. Rev.* **2010**, *254*, 1713.
(5) (a) Jin, Y.; Yoon, I.; Seo, J.; Lee, J.-E.; Moon, S.-T.; Kim, J.; Han, S. W.; Park, K.-M.; Lindoy, L. F.; Lee, S. S. *Dalton Trans.* **2005**, 788. (b) Lee, J.-E.; Jin, Y.; Seo, J.; Yoon, I.; Song, M. R.; Lee, S. Y.; Park, K.-M.; Lee, S. S. *Bull. Korean Chem. Soc.* **2006**, *27*, 203. (c) Seo, J.; Park, S.; Lee, S. S.; Fainerman-Melnikova, M.; Lindoy, L. F. *Inorg. Chem.* **2009**, *48*, 2770.
(6) (a) Lee, E.; Lee, S. S. *Inorg. Chem.* **2011**, *50*, 5803. (b) Park, S.; Lee, S. Y.; Park, K.-M.; Lee, S. S. *Acc. Chem. Res.* **2012**, *45*, 391.
(7) (a) Lee, J. Y.; Kwon, J.; Park, C. S.; Lee, J.-E.; Sim, W.; Kim, J. S.; Seo, J.; Yoon, I.; Jung, J. H.; Lee, S. S. *Org. Lett.* **2007**, *9*, 493. (b) Lee, J. Y.; Kim, H. J.; Jung, J. H.; Sim, W.; Lee, S. S. *J. Am. Chem. Soc.* **2008**, *130*, 13838. (c) Lee, J. Y.; Kim, H. J.; Park, C. S.; Sim, W.; Lee, S. S. *Chem.—Eur. J.* **2009**, *15*, 8989.
(8) (a) *MOGUL*; Cambridge Crystallographic Database: Cambridge: UK, 2006. (b) Lee, S. Y.; Park, S.; Seo, J.; Lee, S. S. *Inorg. Chem. Commun.* **2007**, *10*, 1102. (c) Kim, H. J.; Sultana, K. F.; Lee, J. Y.; Lee, S. S. *CrystEngComm* **2010**, *12*, 1494.
(9) (a) Lee, S. Y.; Seo, J.; Yoon, I.; Kim, C.-S.; Choi, K. S.; Kim, J. S.; Lee, S. S. *Eur. J. Inorg. Chem.* **2006**, 3525. (b) Park, S. B.; Yoon, I.; Seo, J.; Kim, H. J.; Kim, J. S.; Lee, S. S. *Bull. Korean Chem. Soc.* **2006**, *27*, 713.
(10) (a) Adam, K. R.; Arshad, S. P. H.; Baldwin, D. S.; Duckworth, P. A.; Leong, A. J.; Lindoy, L. F.; McCool, B. J.; McPartlin, M.; Tailor, B. A.; Tasker, P. A. *Inorg. Chem.* **1994**, *33*, 1194. (b) Doerrer, L. H.; Lippard, S. J. *Inorg. Chem.* **1997**, *36*, 2554. (c) Park, K.-M.; Moon, S.-T.; Kang, Y. J.; Kim, H. J.; Seo, J.; Lee, S. S. *Inorg. Chem. Commun.* **2006**, *9*, 671. (d) Choi, K. S.; Kang, D.; Lee, J.-E.; Seo, J.; Lee, S. S. *Bull. Korean Chem. Soc.* **2006**, *27*, 747.
(11) (a) Adam, K. R.; Baldwin, D. S.; Duckworth, P. A.; Lindoy, L. F.; McPartlin, M.; Bashall, A.; Powell, H. R.; Tasker, P. A. *J. Chem. Soc., Dalton Trans.* **1995**, 1127. (b) Ghosh, P.; Wood, M.; Bonanno, J. B.; Hascall, T.; Parkin, G. *Polyhedron* **1999**, *18*, 1107. (c) Zhang, Y.; Jianmin, L.; Nishiura, M.; Hou, H.; Deng, W.; Imamoto, T. *J. Chem. Soc., Dalton Trans.* **2000**, 293.
(12) (a) McAuley, A.; Subramanian, S. *Inorg. Chem.* **1990**, *29*, 2830. (b) Vries, N.; Reedijk, J. *Inorg. Chem.* **1991**, *30*, 3700. (c) Chandrasekhar, S.; McAuley, A. *Inorg. Chem.* **1992**, *31*, 2234. (d) Kang, D.; Park, K.-M.; Lee, S. Y.; Lee, S. S.; Choi, K. S. *Bull. Korean Chem. Soc.* **2007**, *28*, 2546.
(13) Lee, J.-E.; Kim, H. J.; Lee, S. Y.; Lee, J. Y.; Jin, Y.; Lee, S. S. *Bull. Korean Chem. Soc.* **2007**, *28*, 2041.
(14) Vaiana, L.; Platas-Iglesias, C.; Esteban-Gómez, D.; Avecilla, F.; de Blas, A.; Rodríguez-Blas, T. *Eur. J. Inorg. Chem.* **2007**, 1874.
(15) *APEX2 Version 2009.1−0 Data Collection and Processing Software*; Bruker AXS Inc.: Madison, Wisconsin, USA, 2008.
(16) *SHELXTL-PC Version 6.22 Program for Solution and Refinement of Crystal Structures*; Bruker AXS Inc.: Madison, Wisconsin, USA, 2008.